

U. (Balu) Balachandran · Beihai Ma

## Mixed-conducting dense ceramic membranes for air separation and natural gas conversion

Received: 10 December 2005 / Accepted: 18 December 2005 / Published online: 23 March 2006  
© Springer-Verlag 2006

**Abstract** Non-perovskite  $\text{SrFeCo}_{0.5}\text{O}_x$  (SFC2) was found to have high electronic and ionic conductivities as well as structural stability. At 800 °C in air, total and ionic conductivities of 17 and 7  $\text{S}\cdot\text{cm}^{-1}$  were measured, respectively; the ionic transference number was calculated to be  $\approx 0.4$ . This material is unique because of its high electronic conductivity and comparable electronic and ionic transference numbers. X-ray diffraction analysis showed that air-sintered SFC2 consists of three phase components,  $\approx 75$  wt%  $\text{Sr}_4(\text{Fe}_{1-x}\text{Co}_x)_6\text{O}_{13\pm\delta}$ ,  $\approx 20$  wt% perovskite  $\text{Sr}(\text{Fe}_{1-x}\text{Co}_x)\text{O}_{3-\delta}$ , and  $\approx 5$  wt% rock salt  $\text{CoO}$ . Argon-annealed SFC2 contains brownmillerite  $\text{Sr}_2(\text{Fe}_{1-x}\text{Co}_x)_2\text{O}_5$  and rock salt  $\text{CoO}$ . Dense SFC2 membranes were able to withstand large  $\text{pO}_2$  gradients and retain mechanical strength. A 2.9-mm-thick disk membrane was tested in a gas-tight electrochemical cell at 900 °C; an oxygen permeation flux rate  $\approx 2.5 \text{ cm}^3(\text{STP})\cdot\text{cm}^{-2}\cdot\text{min}^{-1}$  was measured. A dense thin-wall tubular membrane of 0.75-mm thickness was tested in a methane conversion reactor for over 1,000 h. At 950 °C, the oxygen permeation flux rate was  $\approx 10 \text{ cm}^3(\text{STP})\cdot\text{cm}^{-2}\cdot\text{min}^{-1}$  when the SFC2 thin-wall membrane was exposed with one side to air and the other side to 80% methane balanced with inert gas. Results from these two independent experiments agreed well. The SFC2 material is a good candidate as dense ceramic membranes for oxygen separation from air or for use in methane conversion reactors.

**Keywords** Mixed conductor · Membrane · Oxygen permeability · Oxygen ionic conductivity

### Introduction

Mixed-conducting oxides that exhibit both electronic and oxygen ionic conduction have found wide application in high temperature solid-state electrochemical devices such as solid-oxide fuel cells, batteries, and sensors. These materials also hold particular promise in dense ceramic membrane technology for separation of oxygen from air. In recent years, the development in dense ceramic membrane technology has accelerated. This technology enabled the combination of oxygen separation from air and partial oxidation of natural gas in a single unit. By eliminating the need for a separate oxygen production plant, the technology significantly reduces the energy and capital cost associated with production of synthesis gas (syngas,  $\text{CO}+\text{H}_2$ ), which is an important intermediate in the production of hydrogen and the conversion of methane to value-added products [1, 2]. The successful development of this technology would provide a substantial and more cost-competitive source of cleaner burning energy compared to conventional fuels.

Progress in dense ceramic membrane technology has benefited from the development of mixed-conducting oxides. Metallic oxides, such as zirconia, are unsuitable for a commercial oxygen separator because of the lack of electronic conduction in such materials. They require external electrical circuitry, which makes the system impractical. Incorporation of dopants such as  $\text{TiO}_2$ ,  $\text{Pr}_2\text{O}_3$ , or  $\text{Eu}_2\text{O}_3$  to increase the electronic conductivity in zirconia met with limited success in creating an “electrode-less” membrane material [3–5]. An alternative approach is to use perovskites of the  $\text{ABO}_3$  type with doping on the “A” or “B” site. After the discovery by Teraoka et al. [6, 7] in the late 1980s, mixed-conducting perovskites of  $(\text{La},\text{Sr})(\text{Fe},\text{Co})\text{O}_3$  system, which exhibit both electronic and oxygen ionic conductivities and appreciable oxygen permeability, attracted great attention [8–16].

Ceramic materials that exhibit combined high electronic and oxygen ionic conductivities are of particular interest. These materials not only transport oxygen ions (i.e., function as a selective oxygen separator) but also transport electrons back from the catalytic side of the reactor

U. (B.) Balachandran (✉) · B. Ma  
Energy Technology Division, Argonne National Laboratory,  
9700 South Cass Avenue,  
Argonne, IL 60439, USA  
e-mail: balu@anl.gov  
Tel.: +1-630-2524250  
Fax: +1-630-2523604

membrane to the oxygen reduction interface. As such, no external electrodes are required if the driving force (electrochemical potential) is sufficient and the partial oxidation reaction should be spontaneous. Such a system will operate without an externally applied potential. Oxygen is transported across the ceramic membrane material in the form of anions rather than molecules. The dense membrane material can be shaped into a hollow tube reactor, with air passed through the inside of the membrane and methane through the outside, as shown in Fig. 1. The membrane is permeable to oxygen at high temperature, but not to nitrogen and other gases. Thus, only oxygen from air can be transported through the membrane to react with methane, producing syngas.

The perovskite  $(\text{La},\text{Sr})(\text{Fe},\text{Co})\text{O}_3$  has good electronic and ionic conductivities in an oxygen-rich environment. Electronic conductivity of  $\sigma_{\text{el}}=76 \text{ S}\cdot\text{cm}^{-1}$  and ionic conductivity of  $\sigma_{\text{ion}}=4 \text{ S}\cdot\text{cm}^{-1}$  were measured on  $\text{SrFe}_{0.2}\text{Co}_{0.8}\text{O}_{3-\delta}$  (SFC1), at 800 °C in air [17]. In addition, a high oxygen flux of  $\approx 3 \text{ cm}^3(\text{STP})\cdot\text{cm}^{-2}\cdot\text{min}^{-1}$  was reported being measured at 875 °C on a 1-mm-thick disk with one side exposed to helium and the other side to air [6]. However, SFC1 lacks structural stability when exposed to large gradients of the oxygen partial pressure ( $p\text{O}_2$ ) [18, 19]. This condition makes it unsuitable for use as a dense ceramic membrane in the partial oxidation of methane to form syngas. Adding a small amount of  $\text{ZrO}_2$  into SFC1 to stabilize its structure and to enhance its mechanical properties and oxygen permeability in a low  $p\text{O}_2$  environment had limited success [20, 21].

A non-perovskite mixed-conducting oxide,  $\text{SrFeCo}_{0.5}\text{O}_{3\pm\delta}$  (SFC2), was found to have not only higher oxygen permeability but also structural stability in both oxidizing and reducing environments [22–25]. In this article, we re-

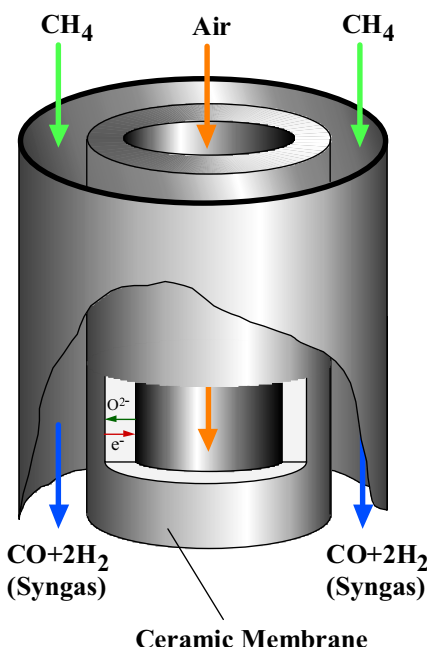


**Fig. 1** Schematic drawing of oxygen-permeable ceramic membrane used in methane conversion reactor

port processing and fabrication of hollow SFC2 membrane tubes for use in methane oxidation reactors. Room-temperature powder X-ray diffraction and scanning electron microscopy (SEM) were conducted to characterize the materials. Extruded hollow tubes of SFC2 were evaluated in the cell operating at  $\approx 900$  °C for conversion of methane into syngas. Electronic and oxygen ionic conductivities and oxygen permeability of SFC2 material will be discussed.

## Experimental

### Sample preparation

$\text{SrFeCo}_{0.5}\text{O}_{3\pm\delta}$  (SFC2) powder was made by solid-state reaction with appropriate amounts of  $\text{SrCO}_3$ ,  $\text{Co}(\text{NO}_3)_2\cdot 6\text{H}_2\text{O}$ , and  $\text{Fe}_2\text{O}_3$ ; mixing and ball milling were done in isopropanol with zirconia grinding medium for 15 h. After drying, the mixture was calcined in air at 850 °C for 16 h, with intermittent grinding. After the final calcination, the powder was ground with an agate mortar and pestle to an average size of  $\approx 7 \mu\text{m}$ , and the resulting powder was pressed with a 120-MPa load into pellets of  $\approx 21$ -mm diameter and  $\approx 3$ -mm thickness. The pressed pellets were covered by powder of the same composition to eliminate contamination and then sintered at  $\approx 1200$  °C in air for 5 h. The bulk density of the sintered sample was determined by the Archimedean method. For four-probe conductivity experiments, thin bars were cut from the air-sintered pellets. For oxygen permeation studies, pellets were polished on both sides and finished with 600-grade SiC grinding paper.

To fabricate the hollow-tube membranes by plastic extrusion, the calcined powder is mixed with several organic additives to provide enough plasticity for easy forming into various shapes while retaining satisfactory strength in the green state (before firing). This formulation, generally known as a slip, consists of a solvent, dispersant, binder, plasticizer, and ceramic powder. After the slip is prepared, some of the solvent was allowed to evaporate; this yields a plastic mass that was forced through a die to produce hollow tubes. Tubes have been extruded with an outer diameter of  $\approx 6.5$  mm and length up to 30 cm. Wall thicknesses are 0.25 to 1.20 mm. The extruded tubes are heated slowly at  $\approx 5$  °C/h in the temperature range between 150 and 400 °C to facilitate removal of gaseous species formed during decomposition of the organic additives. After the organics are removed, the heating rate is increased to  $\approx 60$  °C/h, and the tubes are sintered at 1,200 °C for 5 to 10 h in air. Post-annealing treatment was conducted in flowing argon ( $p\text{O}_2 \approx 10^{-6}$  atm) at 1,100 °C for 48 h.

### Sample characterization

Room-temperature powder X-ray diffraction data were collected with a Scintag XDS-2000 diffractometer, using  $\text{Cu}(K\alpha_1)$  radiation. A high-purity intrinsic Ge energy-dispersive detector was used to minimize background due

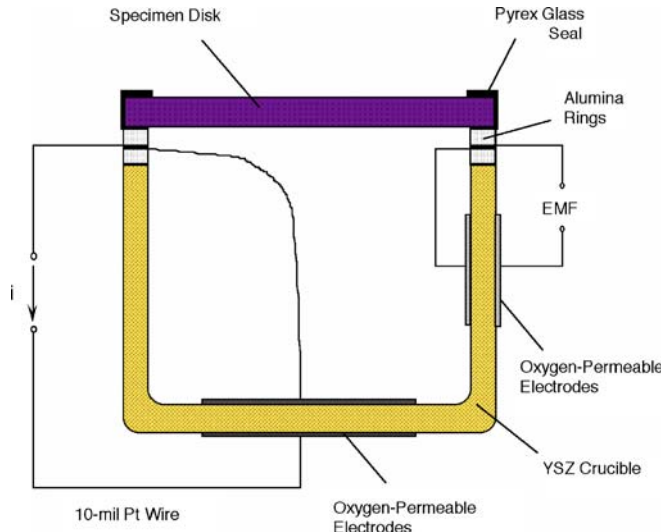


**Fig. 2** Schematic drawing of gas-tight electrochemical cell used to measure oxygen permeability

to sample fluorescence. A continuous scan, with a  $2\theta$  scanning rate of  $1^\circ \text{ min}^{-1}$  and step of  $0.03^\circ$ , was used to collect data. Rietveld analysis [26] of the X-ray diffraction data was performed by means of the General Structure Analysis System suite of programs [27]. SEM observations were conducted with a JEOL JSM-5400 scanning microscope at an accelerating voltage of 20 keV. The theoretical density of SFC2 was measured on a powder sample with an AccuPyc 1330 pycnometer and was confirmed by X-ray powder diffraction. The bulk density of the samples used in our experiments was  $\approx 95\%$  of the theoretical value.

Total conductivity of the sample was determined by the conventional four-probe method, and ionic conductivity was measured with the electron-blocking method. Platinum wires were attached to the specimen bar to serve as current and voltage leads. Resistance of the specimen was measured with an HP 4192A LF impedance analyzer at 23 Hz. Details of the experimental configuration for

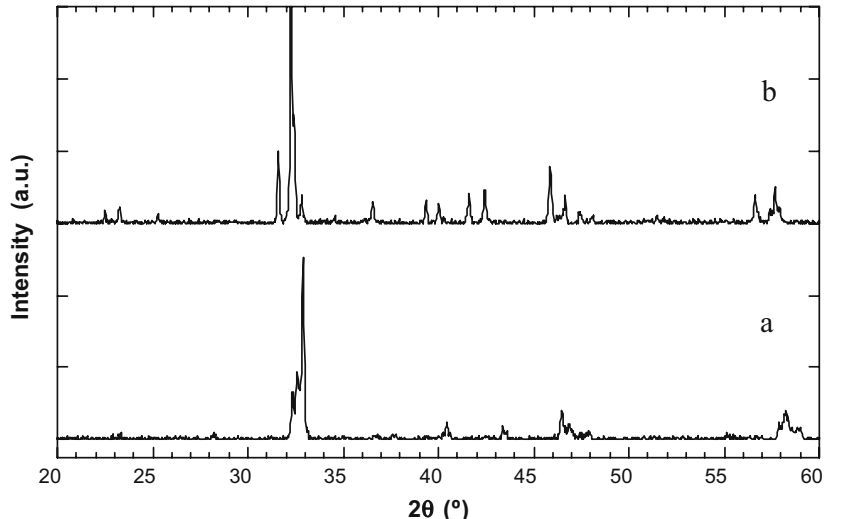
measuring conductivity were reported earlier [17]. A K-type thermocouple was attached to an yttria-stabilized zirconia (YSZ) plate, on which sample bars were placed for testing. The thermocouple was used for both controlling and detecting the temperature of the electric furnace. Temperature tolerance within the uniform hot zone of the furnace is  $\pm 1^\circ \text{C}$ . Desirable gaseous environments were obtained by flowing premixed gases through the system during the experiments.

Figure 2 shows a schematic diagram of the gas-tight electrochemical cell used in the oxygen permeation experiments. A sintered pellet of SFC2 was sealed to a YSZ crucible with a Pyrex glass seal. Electrical leads (10-mil Pt wires) were separated from the YSZ crucible and SFC2 disk membrane by two alumina rings. Electrodes were made on the bottom and side wall of the YSZ crucible. The bottom electrodes were used as pumping electrodes, to pump oxygen from the gas-tight cell chamber, whereas the other electrodes were used to detect the  $pO_2$  inside the cell. The  $pO_2$  inside the cell can be determined from the electromotive force (EMF),  $E$ , generated on the side wall of the YSZ crucible by solving

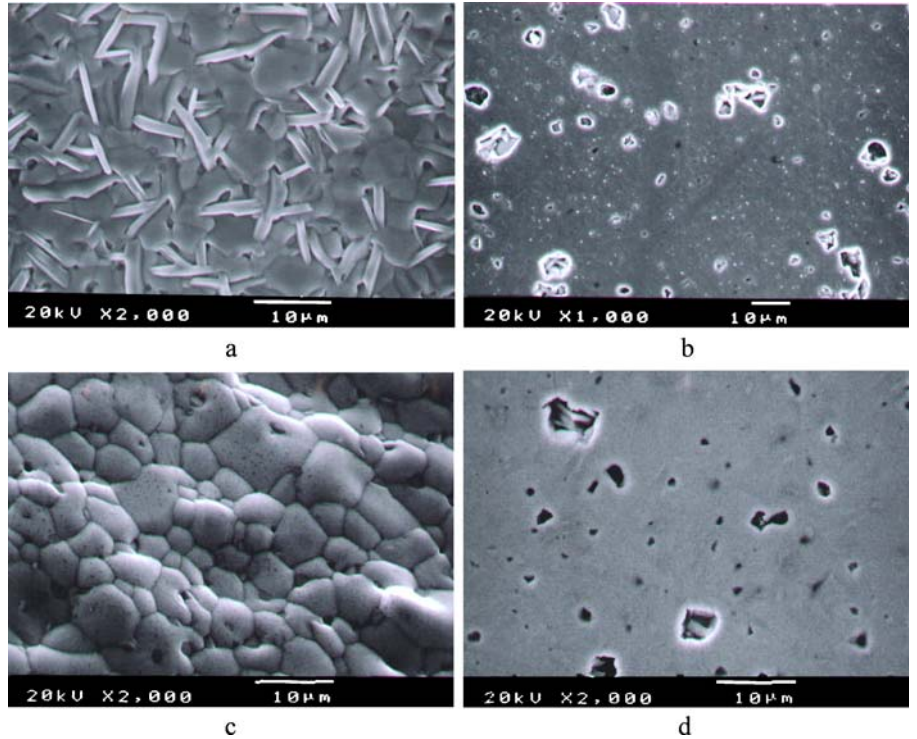
$$pO_2^{II} = pO_2^I \exp \left( \frac{4F \cdot E}{RT} \right), \quad (1)$$

where  $pO_2^{II}$  and  $pO_2^I$  are the  $pO_2$  values inside and outside the gas-tight cell, respectively. Other variables are as usual:  $F$ , Faraday's constant;  $R$ , gas constant; and  $T$ , absolute temperature. Reduced- $pO_2$  environments were achieved by pumping oxygen from the gas-tight cell by using the pumping electrodes on the YSZ crucible. Oxygen permeates through the SFC2 disk membrane because of the  $pO_2$  difference on the two sides of the membrane. Under steady-state conditions, the amount of oxygen that enters the cell by permeating the specimen disk is equal to that pumped out by the YSZ oxygen pump. Therefore, the flow of oxygen through the specimen can be determined from the current applied to the YSZ oxygen pump. The

**Fig. 3** Room-temperature X-ray diffraction profiles of the **a** air-sintered and **b** argon-annealed SFC2 sample



**Fig. 4** SEM morphology of SFC2 sample: **a** original surface and **b** polished surface of air-sintered sample; **c** original surface and **d** polished surface of argon-annealed sample



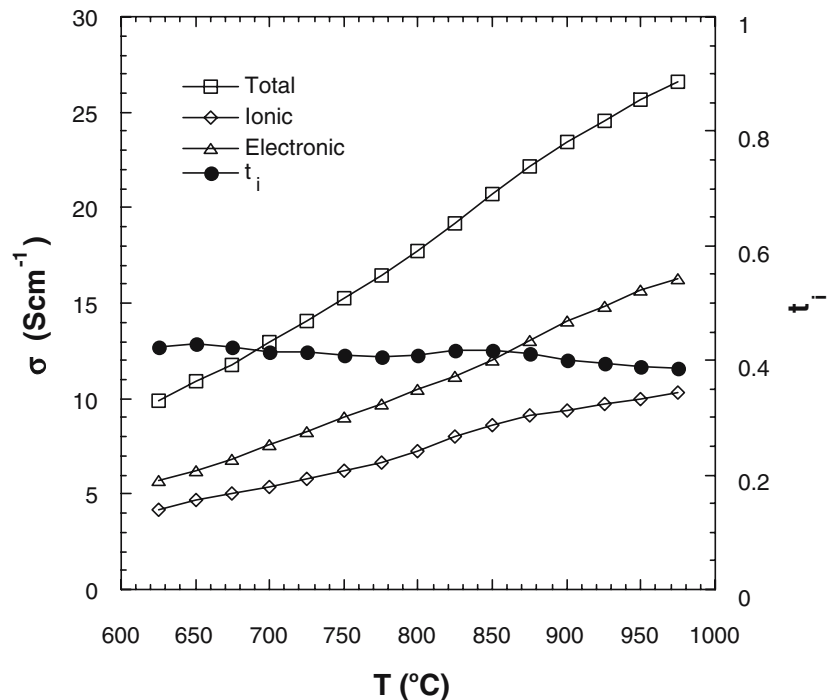
relationship of oxygen permeation flux  $jO_2$  (in mole per square centimeter per second) to the applied current  $I$  (in amperes) is given by:

$$jO_2 = \frac{I}{4F \cdot S}, \quad (2)$$

where  $S$  is the effective cross-sectional area of the specimen.

**Fig. 5** Temperature dependence of conductivities, corresponding to left  $y$ -axis; and ionic transference number, corresponding to right  $y$ -axis of SFC2 in air

The tubular SFC2 membranes were evaluated for performance in a reactor system reported earlier [19]. The quartz tubes support the ceramic membrane tube with hot Pyrex seals. This design allows the equilibration of gases in the reactor. An Rh-based reforming catalyst was loaded adjacent to the tube, and a gold wire mesh was wrapped around the SFC2 tube to prevent solid-state reactions occurring between the catalyst and the ceramic tube. Both the feed gas (80% methane balanced with inert



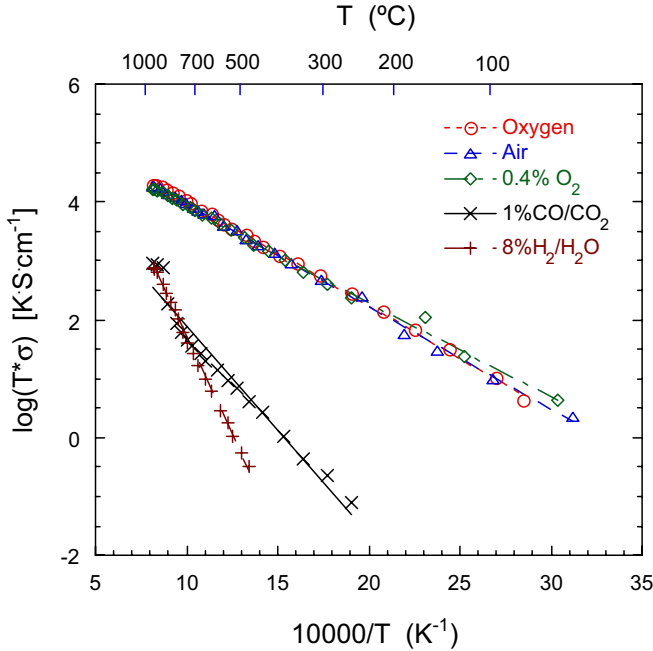


**Fig. 6** Log( $T\sigma$ ) as a function of reciprocal temperature under various pO<sub>2</sub> levels

gas, helium or argon) and the effluents were analyzed by gas chromatography.

## Results and discussions

Figure 3 shows room-temperature X-ray powder diffraction profiles of the air-sintered (Fig. 3a) and argon-annealed (Fig. 3b) SFC2 materials. For the air-sintered SFC2, Rietveld profile analysis of the diffraction data revealed a multi-phase composition of approximately 70 wt% (weight percent) non-perovskite  $Sr_4(Fe_{1-x}Co_x)_6O_{13\pm\delta}$ , 25 wt% perovskite  $Sr_4(Fe_{1-y}Co_y)O_{3-\delta}$ , and 5 wt% rock salt CoO

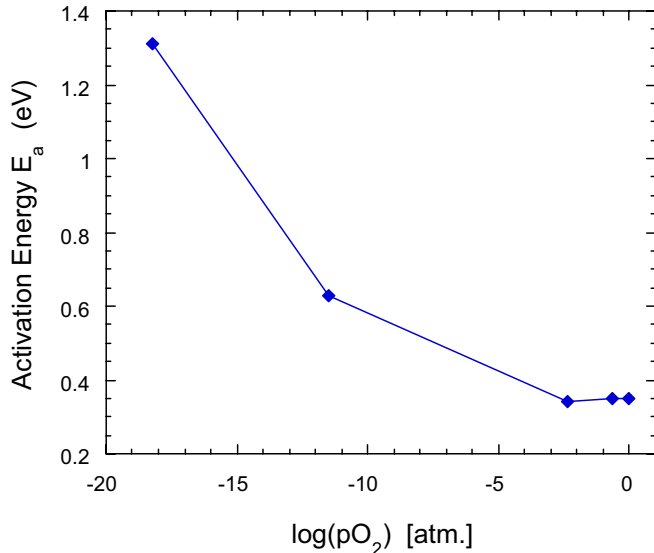


**Fig. 7** Activation energy as a function of pO<sub>2</sub> for SFC2

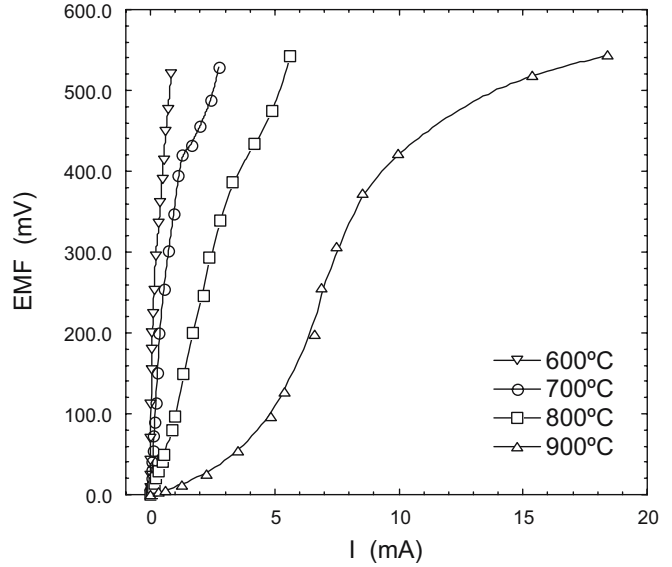
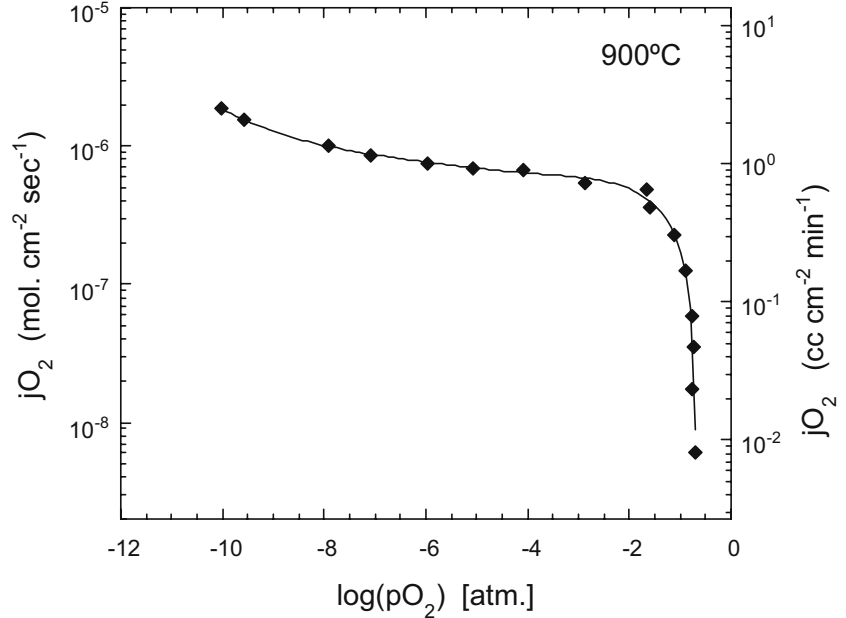


**Fig. 8** Electromotive force of SFC2 as a function of the pumping current at various temperatures for a specimen of 2.9-mm thickness

[28]. A lattice parameter of  $a=4.262$  Å was determined for the CoO phase present in this air-sintered SFC2 sample. Comparison with reported lattice parameters for CoO and FeO, possessing the rock salt crystal structure, of  $a=4.260$  and 4.307 Å [29], respectively, indicates that little, <8%, or no substitution by iron has occurred in the component CoO phase. Lattice parameters determined from Rietveld analysis for the  $Sr_4(Fe_{1-x}Co_x)_6O_{13\pm\delta}$  phase are  $a=11.017$  Å,  $b=19.008$  Å,  $c=5.562$  Å, and cell volume  $V=1169.8$  Å<sup>3</sup>. These values compare well with those reported by Guggilla and Manthiram [30]. As for the argon-annealed SFC2, it contains brownmillerite  $Sr_2(Fe_{1-x}Co_x)_2O_5$  and rock salt CoO [31]. Although the crystalline structure of the air-sintered SFC2 changes after annealing in a reducing atmosphere, its mechanical integrity retained when a disk or hollow-tube membrane of SFC2 is exposed to a large pO<sub>2</sub> gradient, such as is the case with one side exposed to air and the other side to a highly reducing atmosphere (80% methane balanced with inert gas). In contrast, the perovskite  $Sr(Fe, Co)O_{3-\delta}$  (SFC1) loses its mechanical integrity and cracks into pieces due to large lattice parameter changes after exposure to a highly reducing environment. Its superior mechanical structural stability in both oxidizing and reducing atmospheres makes SFC2 a potential material for use as dense ceramic membranes for oxygen separation from air or use in methane conversion reactors.

SEM images of the air-sintered and argon-annealed SFC2 sample are shown in Fig. 4; they reveal a dense structure for both samples. Energy-dispersive X-ray elemental analysis showed that the overall atomic ratio of the metal elements is consistent with that given in the nominal chemical formula for SFC2,  $SrFeCo_{0.5}O_{3\pm\delta}$ . The polished surface SEM images showed that the argon-annealed sample is denser and contains fewer pores than the

**Fig. 9** Oxygen permeation flux rate of SFC2 as a function of oxygen potential at 900 °C for a specimen of 2.9-mm thickness



air-sintered sample. A spherical cobalt-rich phase of CoO was observed in the argon-annealed sample.

The total conductivity ( $\sigma_{\text{tot}}$ ), ionic conductivity ( $\sigma_{\text{ion}}$ ), electronic conductivity ( $\sigma_{\text{el}}$ ), and ionic transference number ( $t_i = \sigma_{\text{ion}}/\sigma_{\text{tot}}$ ) are plotted in Fig. 5 as a function of temperature. Total, ionic, and electronic conductivities all increase linearly with increasing temperature. The ionic transference number is  $\approx 0.4$ , almost independent of temperature in the range measured. At 800 °C in air, total and ionic conductivities are 17 and 7 S·cm<sup>-1</sup>, respectively.

Figure 6, a plot of  $\log(T\cdot\sigma)$  as a function of reciprocal temperature in various oxygen environments, shows that  $\log(T\cdot\sigma)$  has good linear dependence on reciprocal temperature. The total conductivity of SFC2 increases with increasing

temperature and pO<sub>2</sub>. Empirically, the temperature dependence of the total conductivity can be expressed by

$$\sigma = \frac{A}{T} \exp\left(-\frac{E_a}{RT}\right), \quad (3)$$

where  $A$  is a fitting constant,  $E_a$  activation energy,  $R$  gas constant, and  $T$  absolute temperature. The activation energy of SFC2 was calculated from the slopes of  $\log(T\cdot\sigma)$  vs  $10,000/T$  curves using Eq. 3.  $E_a$  thus determined is plotted in Fig. 7 as a function of pO<sub>2</sub>. The activation energy increases with decreasing pO<sub>2</sub> in the low-pO<sub>2</sub> range ( $< 10^{-3}$  atm), whereas in the high-pO<sub>2</sub> range ( $> 10^{-3}$  atm), activation energy is independent of pO<sub>2</sub> and has a lower value ( $\approx 0.35$  eV) compared to those perovskite  $Sr(Fe, Co)O_{3-\delta}$  systems [32, 33].

The setup shown in Fig. 2 was used to measure the oxygen permeability of SFC2 in the presence of a steady flow of oxygen through the disk specimen within a temperature range of 600–900 °C. During the experiment, the gas-tight cell was surrounded with flowing air. pO<sub>2</sub> inside the cell was controlled by the applied pumping current, the value of which was determined by measuring the EMF generated on sensor electrodes and solving Eq. 1. When oxygen had been pumped out from the cell, the specimen disk was in an oxygen chemical potential gradient, with one side exposed to air ( $pO_2=0.21$  atm), and the other side exposed to a reducing atmosphere. Therefore, oxygen was incorporated into the specimen from the high-pO<sub>2</sub> side, moved under the oxygen chemical potential gradient, then left the specimen and entered the gas-tight cell. The dependence of EMF on the sensor electrodes as a function of pumping current  $I$  is plotted in Fig. 8 for a specimen of 2.9-mm thickness. At low temperature, EMF measured from the oxygen sensor exhibits nearly linear dependence on pumping current. Oxygen

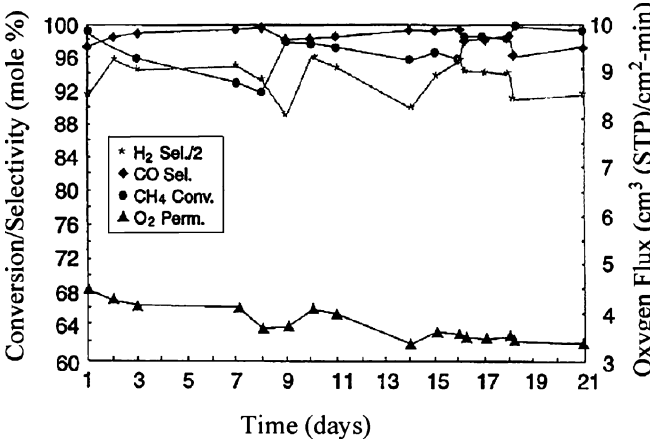
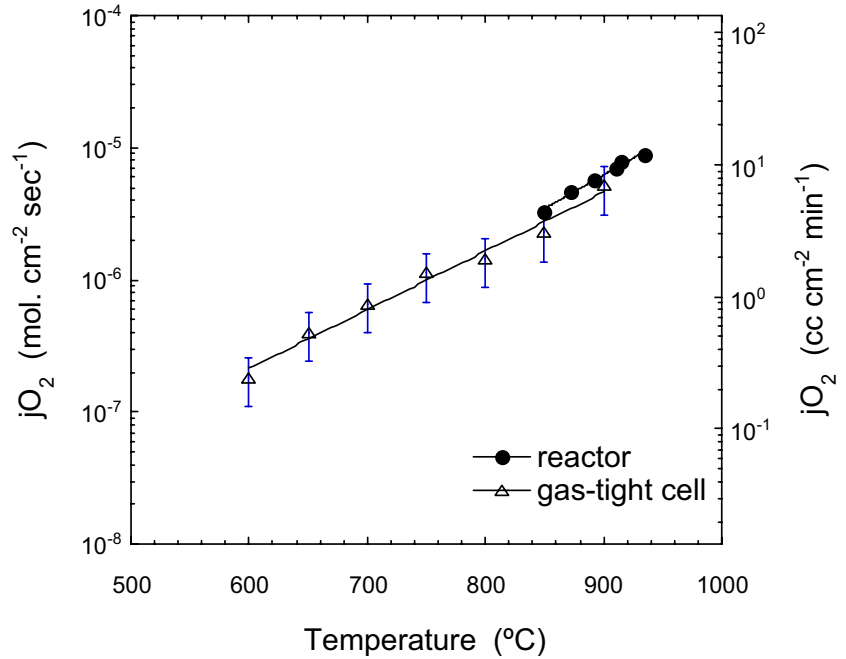


**Fig. 10** Methane conversion, CO and H<sub>2</sub> selectivities, and oxygen permeation in an SFC2 membrane reactor operated with reforming catalyst for 21 days at 900 °C (80% CH<sub>4</sub>/20% Ar feed, pressure  $\approx 1$  atm)

**Fig. 11** Temperature-dependent oxygen permeation flux determined by two independent methods: gas-tight electrochemical cell and methane conversion reactor



permeability  $jO_2$ , determined by solving Eq. 2 with steady pumping current  $I$  and geometric parameters of the specimen disk, is plotted in Fig. 9 as a function of  $pO_2$  at 900 °C. In this plot of  $jO_2$  vs  $\log(pO_2)$ ,  $jO_2$  increases dramatically within the  $pO_2$  range of 0.21 to  $10^{-3}$  atm, and its slope becomes flat when  $pO_2$  inside the cell is decreased further. At 900 °C, measured oxygen permeability was  $\approx 2.5 \text{ cm}^3 (\text{STP}) \cdot \text{cm}^{-2} \text{ min}^{-1}$  for a 2.9-mm-thick disk specimen when one side of the SFC2 disk was exposed to air and the other side to a reducing ( $pO_2 \approx 10^{-10}$  atm) environment.

Sintered thin-wall, hollow-tube membranes of SFC2 were tested in a methane conversion reactor for over 1,000 h [19, 23, 34]. Data obtained with the reactor using an SFC2 membrane tube are plotted in Fig. 10. The fuel (80% methane, 20% argon) was fed at  $\approx 1$  atm pressure along the shell side of the SFC2 tube. Air at ambient pressure was passed through the inside of the tube. Oxygen from air was selectively transported through the membrane, where it reacted with methane in the presence of the reforming catalyst to produce syngas. This eliminates the need for an expensive oxygen plant. High methane conversion efficiency ( $\approx 98\%$ ) and high CO selectivity ( $> 96\%$ ) were observed. This reactor was deliberately shut down after 21 days. To further confirm the stability of the SFC2 membrane, we operated another reactor with a feed gas that contained CH<sub>4</sub>, CO, CO<sub>2</sub>, and H<sub>2</sub> over a period of 1,000 h [19]. Again, methane conversion efficiency was high. However, the oxygen flux during this operation slowly decreased from  $\approx 4$  to  $\approx 2 \text{ cm}^3 (\text{STP}) \cdot \text{cm}^{-2} \cdot \text{min}^{-1}$ . This is due to the reaction between the reforming catalyst and SFC2 tube. In another experiment, when the reforming catalyst was physically separated from the SFC2 membrane, no noticeable degradation in oxygen flux was observed. To use the SFC2 membrane tube in converting methane to syngas, it appears critical to reduce the wall thickness. A thin-wall membrane will increase the oxygen

flux across the membrane and maximize the surface-area-to-volume ratio, and thereby reduce the required reactor size.

Oxygen permeation flux rates determined from a reactor experiment with tubular SFC2 membranes [35] and from the gas-tight cell experiments are plotted in Fig. 11 as a function of temperature. Oxygen permeability increases with increasing temperature and decreasing membrane wall thickness. The wall thickness of the tubular membrane used in the methane conversion reactor was 0.75 mm. At 950 °C, an oxygen permeation flux of  $\approx 10 \text{ cm}^3 (\text{STP}) \cdot \text{cm}^{-2} \cdot \text{min}^{-1}$  was measured on a hollow-tube SFC2 membrane being operated for over 1,000 h with one side exposed to air and the other side exposed to gas environment of 80% methane balanced with inert gas ( $pO_2 \approx 10^{-22}$  atm). The oxygen permeation flux determined from the gas-tight electrochemical cell was normalized to that for a 0.75-mm-thick membrane for comparison with the data obtained for the methane conversion reactor. As shown in Fig. 11, results from these two independent experiments are in good agreement.

## Conclusions

Mixed-conducting SFC2 exhibits not only high combined electronic and ionic conductivities but also structural stability in both oxidizing and reducing environments. At 800 °C in air, total and ionic conductivities are 17 and  $7 \text{ S} \cdot \text{cm}^{-1}$ , respectively, and the ionic transference number is  $\approx 0.4$ . This material is unique because of its high electrical conductivity and comparable ionic and electronic transference numbers. X-ray diffraction analysis showed that air-sintered SFC2 consists of three phase components: 75 wt%  $Sr_4(Fe_{1-x}Co_x)_6O_{13\pm\delta}$ , 20 wt% perovskite  $Sr(Fe_{1-x}Co_x)$

$O_{3-\delta}$ , and  $\approx 5$  wt% rock salt CoO. Argon-annealed SFC2 contains brownmillerite  $Sr_2(Fe_{1-x}Co_x)_2O_5$  and rock salt CoO. Dense ceramic membranes made of SFC2 can sustain large  $pO_2$  gradients and retain mechanical strength. Therefore, this material is a good candidate for dense ceramic membranes for separation of oxygen from air or use in methane conversion reactors.

The total conductivity of SFC2 measured in air and various reducing environments showed good linear dependence on reciprocal temperature. Total conductivity increased with increasing temperature and  $pO_2$ . Activation energy increased with decreasing  $pO_2$ . In high  $pO_2$  atmosphere, the activation energy ( $\approx 0.35$  eV) for SFC2 was lower than that of perovskite  $Sr(Fe, Co)O_{3-\delta}$  materials.

The oxygen permeability of dense ceramic membranes made of SFC2 was determined using a gas-tight electrochemical cell and a methane conversion reactor. At  $900\text{ }^{\circ}\text{C}$ , oxygen permeation flux rate was  $\approx 2.5\text{ cm}^3(\text{STP})\cdot\text{cm}^{-2}\cdot\text{min}^{-1}$  for a 2.9-mm-thick disk membrane with one side exposed to air and the other side to a  $pO_2 \approx 10^{-10}$  atm environment. A dense thin-wall tubular membrane of 0.75-mm thickness was tested in a methane conversion reactor. High methane conversion efficiency ( $\approx 98\%$ ) and high CO selectivity ( $> 96\%$ ) were observed. At  $950\text{ }^{\circ}\text{C}$ , an oxygen permeation flux of  $\approx 10\text{ cm}^3(\text{STP})\cdot\text{cm}^{-2}\cdot\text{min}^{-1}$  was measured when the hollow-tube SFC2 membrane was exposed with one side to air and the other side to gas environment of 80% methane balanced with inert gas ( $pO_2 \approx 10^{-22}$  atm). The flux rates measured from these two independent experiments (gas-tight electrochemical cell and methane conversion reactor) are in good agreement.

**Acknowledgement** The work at Argonne is supported by the U.S. Department of Energy, Federal Energy Technology Laboratory's Gasification Technologies Program, under Contract W-31-109-Eng-38.

## References

1. Keller GE, Bhasin MM (1982) *J Catal* 73:9
2. Fierro JGL (1993) *Catal Lett* 22:67
3. Hazbun EA (1988) US Patent 4791079, 13 Dec 1988
4. Gur TM, Belzner A, Huggins RA (1992) *J Membr Sci* 75:151
5. Cable TL (1990) European Patent EP 0399833 A1, 28 Nov 1990
6. Teraoka Y, Zhang H, Furukawa S, Yamazoe N (1985) *Chem Lett* 1985:1743
7. Teraoka Y, Zhang H, Okamoto K, Yamazoe N (1988) *Mater Res Bull* 23:51
8. Nigara Y, Mizusaki J, Ishigame M (1995) *Solid State Ionics* 79:208
9. Arashi H, Naito H, Nakata M (1995) *Solid State Ionics* 76:315
10. Van Doorn RHE, Kruidhof H, Bouwmeester HJM, Burggraaf AJ (1991) *Mater Res Soc Symp Proc* 369:377
11. Teraoka Y, Nobunaga T, Okamoto K, Miura N, Yamazoe N (1991) *Solid State Ionics* 48:207
12. Brinkman HW, Kruidhof H, Burggraaf AJ (1994) *Solid State Ionics* 68:173
13. Balachandran U, Morissette SL, Dusek JT, Mieville RL, Poeppel RB, Kleefisch MS, Pei S, Kobylinski TP, Udovich CA (1993) Proceedings of Coal Liquefaction and Gas Conversion Contractors' Review Conference, vol 1. In: Rogers S (ed) US Dept of Energy, Pittsburgh Energy Technology Center, pp 138–160
14. Shao Z, Yang W, Cong Y, Dong H, Tong J, Xiong G (2000) *J Membr Sci* 172:177
15. Li S, Jin W, Huang P, Xu N, Shi J, Lin YS (2000) *J Membr Sci* 166:51
16. Vente JF, Haije WG, Rak ZS (2004) Inorganic membranes. In: Akin FT, Lin YS (eds) Proceedings of 8th International Conference on Inorganic Membranes. Admas Press, Chicago, pp 595–598
17. Ma B, Park JH, Segre CU, Balachandran U (1995) *Mater Res Soc Symp Proc* 393:49
18. Pei S, Kleefisch MS, Kobylinski TP, Faber J, Udovich CA, Zhang-McCoy V, Dabrowski B, Balachandran U, Mieville RL, Poeppel RB (1995) *Catal Lett* 30:201
19. Balachandran U, Dusek JT, Mieville RL, Poeppel RB, Kleefisch MS, Pei S, Kobylinski TP, Udovich CA, Bose AC (1995) *Appl Catal A* 133:19
20. Li SG, Jin WQ, Huang P, Xu NP, Shi J, Hu ZC, Payzant EA, Ma YH (1999) *AIChE J* 45:276
21. Yang L, Gu XH, Tan L, Jin WQ, Zhang LX, Xu NP (2001) *Ind Eng Chem Res* 41:4273
22. Balachandran U, Kleefisch MS, Kobylinski TP, Morissette SL, Pei S (1994) International Patent WO96/24065
23. Balachandran U, Dusek JT, Sweeney SM, Poeppel RB, Mieville RL, Maiya PS, Kleefisch MS, Pei S, Kobylinski TP, Udovich CA, Bose AC (1995) *Am Ceram Soc Bull* 74:71
24. Ma B, Balachandran U, Park JH, Segre CU (1996) *J Electrochem Soc* 143:1736
25. Ma B, Balachandran U, Park JH, Segre CU (1996) *Solid State Ionics* 83:65
26. Rietveld HM (1969) *J Appl Crystallogr* 2:65
27. Larson AC, Dreese RB Von (1994) General Structure Analysis System, Los Alamos National Laboratory Internal Report No. 86–748 (1985–1994)
28. Ma B, Hodges JP, Jorgensen JD, Miller DJ, Richardson JW Jr, Balachandran U (1998) *J Solid State Chem* 141:576
29. JCPDS—International Centre for Diffraction Data, No. 9-402 and 6-615
30. Guggilla S, Manthiram A (1997) *J Electrochem Soc* 144:L120
31. Mitchell BJ, Richardson JW Jr, Ma B, Balachandran U (2002) *J European Ceram Soc* 22:661
32. Nisancioglu K, Gur TM (1994) *Solid State Ionics* 72:199
33. Ishigaki T, Yamauchi S, Kishio K, Mizusaki J, Fueki K (1988) *J Solid State Chem* 73:179
34. Balachandran U, Dusek JT, Maiya PS, Ma B, Mieville RL, Kleefisch MS, Udovich CA (1997) *Catal Today* 36:265
35. Maiya PS, Balachandran U, Dusek JT, Mieville RL, Kleefisch MS, Udovich CA (1997) *Solid State Ionics* 99:1